Research Article | Vol. 26, No. 4 | 19 Feb 2018 | OPTICS EXPRESS 4693
Optics EXPRESS

# Design of an ultra-compact graphene-based integrated microphotonic tunable delay line

GIUSEPPE BRUNETTI, DONATO CONTEDUCA, FRANCESCO DELL'OLIO, CATERINA CIMINELLI,* AND MARIO N. ARMENISE

*Optoelectronics Laboratory, Politecnico di Bari, Via E. Orabona 6, 70125, Bari, Italy*
**caterina.ciminelli@poliba.it*

**Abstract:** The design of a continuously tunable optical delay line based on a compact graphene-based silicon Bragg grating is reported. High performance, in terms of electro-optical switching time ($t_{switch}$ < 8 ns), delay range ($\Delta\tau$ = 200 ps), and figure of merit $FOM = \Delta\tau/A$ = 1.54x10$^5$ ps/mm$^2$, has been achieved with an ultra-compact device footprint ($A$ ~1.3 x 10$^{-3}$ mm$^2$), so improving the state-of-the-art of integrated optical delay lines. A continuous and complete tunability of the delay time can be achieved with a very low delay loss ( = 0.03 dB/ps) and a weak power consumption ( = 0.05 mW/ps). A flat bandwidth $B$ = 1.19 GHz has been calculated by exploiting the slow-light effect in the device. This performance makes the proposed optical delay line suitable for several applications in Microwave Photonics (MWP), such as beamsteering/beamforming, for which large delay range, flat and wide bandwidth and small volume are required.



**OCIS codes:** (130.4815) Optical switching devices; (230.3120) Integrated optics devices; (140.4780) Optical resonators.

## References and links

1. J. Capmany and D. Novak, "Microwave photonics combines two worlds," Nat. Photonics **1**(6), 319–330 (2007).
2. J. T. Mok and B. J. Eggleton, "Photonics: Expect more delays," Nature **433**(7028), 811–812 (2005).
3. C. Ciminelli, F. Dell' Olio, and M. N. Armenise, *Photonics in Space* (World Scientific, 2016).
4. J. Yao, "Microwave photonics," J. Lightwave Technol. **27**(3), 314–335 (2009).
5. M. Longbrake, "True time-delay beamsteering for radar," in *IEEE National Aerospace and Electronics Conference NAECON* (2012).
6. T. Tatoli, D. Conteduca, F. Dell'Olio, C. Ciminelli, and M. N. Armenise, "Graphene-based fine-tunable optical delay line for optical beamforming in phased-array antennas," Appl. Opt. **55**(16), 4342–4349 (2016).
7. D. Dolfi, P. Joffre, J. Antoine, J. P. Huignard, D. Philippet, and P. Granger, "Experimental demonstration of a phased-array antenna optically controlled with phase and time delays," Appl. Opt. **35**(26), 5293–5300 (1996).
8. S. Li, X. Li, W. Zou, and J. Chen, "Rangeability extension of fiber-optic low-coherence measurement based on cascaded multistage fiber delay line," Appl. Opt. **51**(6), 771–775 (2012).
9. E. F. Burmeister, J. P. Mack, H. N. Poulsen, M. L. Masanović, B. Stamenić, D. J. Blumenthal, and J. E. Bowers, "Photonic integrated circuit optical buffer for packet-switched networks," Opt. Express **17**(8), 6629–6635 (2009).
10. H. Lee, T. Chen, J. Li, O. Painter, and K. J. Vahala, "Ultra-low-loss optical delay line on a silicon chip," Nat. Commun. **3**(867), 867 (2012).
11. I. Aryanfar, D. Marpaung, A. Choudhary, Y. Liu, K. Vu, D. Y. Choi, P. Ma, S. Madden, and B. J. Eggleton, "Chip-based Brillouin radio frequency photonic phase shifter and wideband time delay," Opt. Lett. **42**(7), 1313–1316 (2017).
12. R. Pant, A. Byrnes, C. G. Poulton, E. Li, D. Y. Choi, S. Madden, B. Luther-Davies, and B. J. Eggleton, "Photonic-chip-based tunable slow and fast light via stimulated Brillouin scattering," Opt. Lett. **37**(5), 969–971 (2012).
13. W. Shi, V. Veerasubramanian, D. Patel, and D. V. Plant, "Tunable nanophotonic delay lines using linearly chirped contradirectional couplers with uniform Bragg gratings," Opt. Lett. **39**(3), 701–703 (2014).
14. N. Ishikura, R. Hosoi, R. Hayakawa, T. Tamanuki, M. Shinkawa, and T. Baba, "Photonic crystal tunable slow light device integrated with multi-heaters," Appl. Phys. Lett. **100**(22), 221110 (2012).
15. X. Wang, L. Zhou, R. Li, J. Xie, L. Lu, K. Wu, and J. Chen, "Continuously tunable ultra-thin silicon waveguide optical delay line," Optica **4**(5), 507–515 (2017).
16. J. Yang, N. K. Fontaine, Z. Pan, A. O. Karalar, S. S. Djordjevic, C. Yang, W. Chen, S. Chu, B. E. Little, and S. J. B. Yoo, "Continuously tunable, wavelength-selective buffering in optical packet switching networks," IEEE Photonics Technol. Lett. **20**(12), 1030–1032 (2008).

#313098 https://doi.org/10.1364/OE.26.004593
Journal © 2018 Received 9 Nov 2017; revised 21 Dec 2017; accepted 14 Jan 2018; published 13 Feb 2018

Optics EXPRESS

17. N. Fontaine, J. Yang, Z. Pan, S. Chu, W. Chen, B. E. Little, and S. J. Ben Yoo, "Continuously tunable optical buffering at 40 gb/s for optical packet switching networks," J. Lightwave Technol. **26**(23), 3776–3783 (2008).
18. A. Melloni, F. Morichetti, C. Ferrari, and M. Martinelli, "Continuously tunable 1 byte delay in coupled-resonator optical waveguides," Opt. Lett. **33**(20), 2389–2391 (2008).
19. P. A. Morton, J. Cardenas, J. B. Khurgin, and M. Lipson, "Fast thermal switching of wideband optical delay line with no long-term transient," IEEE Photonics Technol. Lett. **24**(6), 512–514 (2012).
20. Y. Xie, L. Zhuang, K. J. Boller, and A. J. Lowery, "Lossless microwave photonic delay line using a ring resonator with an integrated semiconductor optical amplifier," J. Opt. **19**(6), 065802 (2017).
21. A. Meijerink, C. G. H. Roeloffzen, R. Meijerink, L. Zhuang, D. A. I. Marpaung, M. J. Bentum, M. Burla, J. Verpoorte, P. Jorna, A. Hulzinga, and W. van Etten, "Novel ring resonator-based integrated photonic beamformer for broadband phased array receive antennas—Part I: design and performance analysis," J. Lightwave Technol. **28**(1), 3–18 (2010).
22. J. Capmany, D. Domenech, and P. Munoz, "Silicon graphene reconfigurable CROWS and SCISSORS," IEEE Photonics J. **7**(2), 1–9 (2015).
23. D. Conteduca, F. Dell'Olio, C. Ciminelli, and M. N. Armenise, "Resonant graphene-based tunable optical delay line," IEEE Photonics J. **7**(6), 1–9 (2015).
24. C. Ciminelli, D. Conteduca, F. Dell'Olio, and M. N. Armenise, "Novel graphene-based photonic devices for efficient light control and manipulation," in *Proceedings in IEEE 17th International Conference on Transparent Optical Networks* (ICTON, 2015).
25. F. Zangeneh-Nejad and R. Safian, "Significant enhancement in the efficiency of photoconductive antennas using a hybrid graphene molybdenum disulphide structure," J. Nanophotonics **10**(3), 036005 (2016).
26. C. T. Phare, Y.-H. D. Lee, J. Cardenas, and M. Lipson, "Graphene electro-optic modulator with 30 GHz bandwidth," Nat. Photonics **9**(8), 511–514 (2015).
27. M. Liu, X. Yin, E. Ulin-Avila, B. Geng, T. Zentgraf, L. Ju, F. Wang, and X. Zhang, "A graphene-based broadband optical modulator," Nature **474**(7349), 64–67 (2011).
28. A. Phatak, Z. Cheng, C. Qin, and K. Goda, "Design of electro-optic modulators based on graphene-on-silicon slot waveguides," Opt. Lett. **41**(11), 2501–2504 (2016).
29. J. Wang, Z. Cheng, Z. Chen, X. Wan, B. Zhu, H. K. Tsang, C. Shu, and J. Xu, "High-responsivity graphene-on-silicon slot waveguide photodetectors," Nanoscale **8**(27), 13206–13211 (2016).
30. F. Xia, T. Mueller, Y.-M. Lin, A. Valdes-Garcia, and P. Avouris, "Ultrafast graphene photodetector," Nat. Nanotechnol. **4**(12), 839–843 (2009).
31. F. Zangeneh-Nejad and R. Safian, "A Graphene-Based THz Ring Resonator for Label-Free Sensing," IEEE Sens. J. **16**(11), 4338–4344 (2016).
32. A. K. Geim and K. S. Novoselov, "The rise of graphene," Nat. Mater. **6**(3), 183–191 (2007).
33. F. Bonaccorso, Z. Sun, T. Hasan, and A. C. Ferrari, "Graphene photonics and optoelectronics," Nat. Photonics **4**(9), 611–622 (2010).
34. M. Liu, X. Yin, and X. Zhang, "Double-layer graphene optical modulator," Nano Lett. **12**(3), 1482–1485 (2012).
35. V. Sorianello, M. Midrio, and M. Romagnoli, "Design optimization of single and double layer Graphene phase modulators in SOI," Opt. Express **23**(5), 6478–6490 (2015).
36. J. Capmany, D. Domenech, and P. Muñoz, "Silicon graphene Bragg gratings," Opt. Express **22**(5), 5283–5290 (2014).
37. Z. Sheng, C. Qiu, H. Li, L. Li, A. Pang, A. Wu, X. Wang, S. Zou, and F. Gan, "Low loss silicon nanowire waveguide fabricated with 0.13 μm CMOS technology," in *Proceedings in IEEE Comm. and Photon. Conference (ACP)* (2012).
38. S. Bae, H. Kim, Y. Lee, X. Xu, J.-S. Park, Y. Zheng, J. Balakrishnan, T. Lei, H. R. Kim, Y. I. Song, Y.-J. Kim, K. S. Kim, B. Özyilmaz, J.-H. Ahn, B. H. Hong, and S. Iijima, "Roll-to-roll production of 30-inch graphene films for transparent electrodes," Nat. Nanotechnol. **5**(8), 574–578 (2010).
39. J. Feng, W. Li, X. Qian, J. Qi, L. Qi, and J. Li, "Patterning of graphene," Nanoscale **4**(16), 4883–4899 (2012).
40. L. A. Coldren, S. W. Corzine, and M. L. Mashanovitch, *Diode Lasers and Photonic Integrated Circuits*, 2nd ed. (John Wiley & Sons, 2012).
41. A. Vakil and N. Engheta, "Transformation optics using graphene," Science **332**(6035), 1291 (2011).
42. F. Z. -Nejad, S. A. Ramezani, K. Arik, and A. Khavasi, "Beam focusing using two-dimensional graphene-based meta-reflect-array," in *2016 24th Iranian Conference on Electrical Engineering* (ICEE, 2016), pp. 613–616.
43. E. Simsek, "A closed-form approximate expression for the optical conductivity of graphene," Opt. Lett. **38**(9), 1437–1439 (2013).

## 1. Introduction

Integrated optical delay lines represent a key element in systems for processing and controlling optical signals. Optical delay lines are essentials in Microwave Photonics to realize chip-scale integrated circuits for several applications, such as filtering, optical buffering and signal correlation, so overcoming the electronics bottlenecks, mainly related to power consumption, large size and weight [1–3].

Optics EXPRESS

The optical beamforming of wideband Phased Array Antennas (PAAs) for telecom and radar payloads in satellite applications represents a promising application in MWP. The features of beams transmitted by PAAs (i.e. direction, amplitude and phase) depend on the amplitude and phase of the RF signal feeding each antenna. In fact, the overall radiation pattern is a combination of the beams radiated by the antenna elements [4,5]. The use of an optical beamforming approach provides an increase of the spatial resolution for Earth observation payloads, and allows to satisfy a large number of user demands at the same time in telecom payloads. The advantages of the optical approach, compared to conventional RF analogue (phase shifters based on loaded or switched lines) or digital beamformers, are more evident for operation at high frequency range, for instance in Ka- or Q-band (frequency > 20 GHz) [3], because the photonic approach enables values of relative bandwidth that are not achievable by the competing technologies.

Typical requirements for optical delay lines used in Synthetic Aperture Radar (SAR) systems for Earth observation applications are a broad bandwidth ($B \geqslant 1$ GHz), wide and continuous delay tunability (delay range in the order of hundreds of picoseconds), fast reconfigurability, and low power consumption [6].

Recently, a strong research effort on tunable optical delay lines has been spent. The most promising devices are based on three main concepts: a long optical path (spiral pattern with either discrete [7,8] or integrated [9,10] configurations), non linear-effects (exploiting third-order non linear response of chalcogenide waveguides [11,12]), and slow light effect.

Resonant true-time delay lines (TTDLs) exploit the slow-light effect in order to provide higher values of optical delay times and large bandwidth. The control of the group velocity allows the tuning of the TTDLs behaviour, so enabling a fine control of the operating conditions. The best performance for this class of devices has been obtained with Bragg gratings [13], Photonic Crystal Waveguides (PhCWs) [14] and Ring Resonators (RRs) [15–17]. These devices have a simple structure, together with a room-temperature operation, although an intrinsic compromise between the maximum delay time, the optical bandwidth and the footprint is necessary. However, these slow-light based devices can ensure large bandwidth up to 100 GHz, with a maximum value of delay time lower than 100 ps [13,17]. Therefore, more complex structures have been proposed in literature to increase the maximum delay time, without sacrificing the bandwidth, such as Coupled-Resonator Optical Waveguides (CROWs) [18], Side-Coupled Integrated Spaced Sequences Of Resonators (SCISSORs) [19], or delay lines obtained by the insertion of an element to compensate the ring resonator loss [20]. Although high values of delay times up to 800 ps for CROW [18] and 345 ps for SCISSOR [19] have been obtained, such devices have a larger footprint (7 $mm^2$ and 0.13 $mm^2$ for the CROW and SCISSOR, respectively). Novel configurations have been proposed to overcome the limitations of the previously reported devices. A continuously tunable optical delay line, based on a ring resonator array and a Mach-Zehnder interferometer switch array was proposed [15], with a continuous delay range of few nanoseconds, wide bandwidth (~60 GHz), but with slow reconfigurability time (> 13 μs). The fast reconfigurability together with a wide and continuous delay range is a crucial aspect of a delay line in optical beamforming applications. High performance in terms of wide and continuous delay range has been demonstrated by using a thermo-optic tuning, although at the expense of a slow response time (> 6 μs) [13, 19, 21]. The electro-optic method is another technique used to realize tunability of optical delay lines, with a much faster response compared to the thermal approach. However, electro-optic approach is typically affected by high values of absorption loss that could be limited only with optimized design and manufacturing technique. Recently, optical delay lines based on the electro-optic tuning realized with a graphene structure have been proposed [6,22–24]. The great interest in graphene is due to its unique optical properties and several graphene-based optical devices have been exploited for several applications, such as antennas [25], optical modulators [26–28], photodetectors [29,30] and optical sensors [31]. In particular, in the field of optical delay

Optics EXPRESS

lines, a strong advantage of graphene is represented by the low value of carrier density of states near the Dirac Point and, therefore, the Fermi energy can be tuned by low values of the applied voltage, so inducing changes in the refractive index that are strong enough to affect the behaviour of the optical delay time [32,33]. Several configurations of graphene-based cascaded ring resonators that can be electro-optically tuned have been proposed. For instance, a continuous time delay range of the order of 200 ps has been achieved in CROWs and SCISSORs with a footprint smaller than 0.1 $mm^2$ [22] and a very fast reconfiguration time of about 0.12 ns, which is five orders of magnitude faster than the typical values obtained by the thermo-optic approach. A fast and continuous delay tuning of approximately 230 ps using two vertically coupled ring resonators interleaved by a graphene capacitor has been reported in [23]. In particular, a bandwidth $B > 1$ GHz, a very small footprint ($1.6 \times 10^{-3}$ $um^2$) and an insertion loss value of 23 dB have been obtained. However, lower values of insertion loss are necessary to avoid an amplification stage at the output of the device.

Here, we propose the design of a delay line based on an ultra-compact one-dimensional photonic crystal (1D-PhC) on SOI technology platform. The grating is obtained by selectively etching in a periodic way a graphene capacitor deposited on the top of a single-mode Si-wire. By applying a voltage to the graphene capacitor, the value of the delay time changes continuously in a wide range ($\Delta\tau > 200$ ps). A maximum delay time of 274.85 ps, together with very small footprint ($A = 1.35 \times 10^{-3}$ $mm^2$), fast reconfigurability and low power consumption have been demonstrated. Furthermore, a flat bandwidth equal to 1.18 GHz has been also obtained, so providing, to our knowledge, the highest value of the figure of merit $FOM = \Delta\tau/A = 1.54 \times 10^5$ ps/$mm^2$ obtained in literature with integrated optical delay lines.

## 2. Device configuration

The optical delay line is based on a Bragg grating made by a periodic pattern of a graphene capacitor on a silicon nanowire, as shown in Fig. 1. The capacitor is realized by two ($t_{gr}$ = 0.34 nm) graphene monolayer electrodes placed on the silicon nanowire, interleaved by a thin layer of $Al_2O_3$ ($n_{Al2O3} = 1.746$ at $\lambda = 1550$ nm), with a thickness $t_{Al} = 7$ nm [23], aiming at enabling the electro-optical tuning of the delay line. The accumulation of the carriers on the graphene layers, corresponding to different values of the electrical conductivity, allows the effective index change in the nanowire. The presence of the graphene capacitor affects the optical losses in the structure. However, the double layer graphene structure provides low values of the insertion loss [34,35], compared to a single layer configuration [36], where the bottom graphene electrode is replaced by a doped silicon layer, with a consequent increase of the optical losses. The silicon nanowire, placed on 2 μm $SiO_2$ substrate, has a cross-section ($n_{Si} = 3.45$ at $\lambda = 1550$ nm), a width, $w_{si}$, equal to 500 nm and a height, $t_{Si}$, equal to 220 nm have been assumed [37] to achieve a single-mode operation. The whole structure is embedded in silica ($SiO_2$) ($n_{SiO2} = 1.444$ at $\lambda = 1550$ nm) (see Fig. 1). The propagation losses of the waveguide without the graphene capacitor at $\lambda = 1550$ nm for the TE mode and the TM mode are $\alpha_{TE} = 2.4$ dB/cm and $\alpha_{TM} = 0.59$ dB/cm, respectively.

A mature manufacturing technique is available to realize the graphene-based photonic silicon Bragg gratings. Large area of a graphene monolayer can be fabricated by Chemical Vapour Deposition (CVD) [38]. The metal deposition can be used to realize the platinum bottom electrode region [27], directly placed on the graphene layer, while the deposition of the $Al_2O_3$ spacer can be done by the Atomic Layer Deposition (ALD), followed by CVD for the deposition of the second monolayer of graphene. Then, a second metal deposition is used for the top electrode. The grating pattern (see Fig. 1), can be achieved with several techniques, such as direct mechanical cleavage, scanning probe lithography, chemical etching or plasma etching [39].

Optics EXPRESS

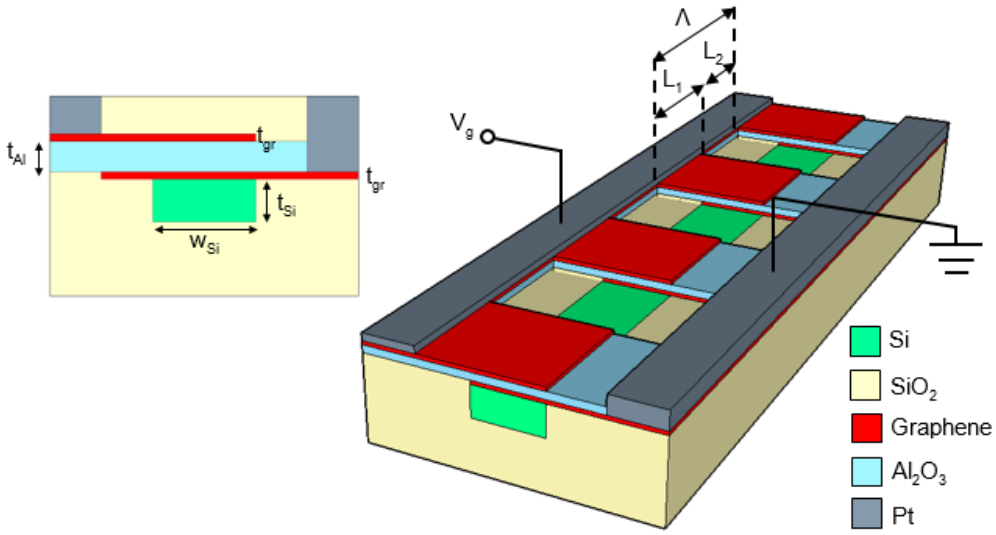


Fig. 1. Configuration of the graphene-based silicon Bragg grating, with the nanowire cross-section in the inset.

## 3. Numerical results

The electromagnetic simulation of the graphene-based silicon Bragg grating has been carried out by the Transmission Matrix Theory (TMT) approach [40]. The TMT is based on the study of a single period of the grating. The matrix product of the single period transmission matrices describes the electromagnetic behaviour of the structure. The *T*-matrix referred to the whole structure is

$$T = \begin{bmatrix} \frac{1}{t^2}\left(e^{j\phi_+} - r^2 e^{-j\phi_-}\right) & \frac{r}{t^2}\left(e^{-j\phi_+} - e^{j\phi_-}\right) \\ \frac{r}{t^2}\left(e^{-j\phi_+} - e^{j\phi_-}\right) & \frac{1}{t^2}\left(e^{-j\phi_+} - r^2 e^{j\phi_-}\right) \end{bmatrix}^N \tag{1}$$

where $r = \left(n_{eff1} - n_{eff2}\right) / \left(n_{eff1} + n_{eff2}\right)$ is the reflection coefficient, $t = \sqrt{1 - r^2}$ is the transmission coefficient, $N$ is the number of the periods and $\phi_\pm = \beta_1 L_1 \pm \beta_2 L_2$ is the phase change. The parameters $\beta_1$, $L_1$ and $n_{eff1}$ are the complex propagation constant (taking into account the structure propagation loss), the length and the effective index, respectively, referred to the region with graphene capacitor, instead the features $\beta_2$, $L_2$ and $n_{eff2}$ are referred to region without graphene capacitor. The *T*-parameters allow to define the *S*-parameters, as described in Eq. (2), that are used to calculate the transmission at the output of the grating [40]:

$$S = \frac{1}{T_{11}} \begin{bmatrix} T_{21} & \det \mathbf{T} \\ 1 & -T_{12} \end{bmatrix} \tag{2}$$

The matrix has been assumed symmetrical in case of linear reciprocal system. By the transmission of the grating ($S_{12}$), the delay time $\tau$ can be evaluated as the derivative of the $S_{12}$ phase ($\angle S_{12}$) with respect to the pulsation ω:

Optics EXPRESS

$$\tau = \frac{\partial\left(\angle S_{12}\right)}{\partial\omega} \tag{3}$$

The fundamental modes of the structures with and without the graphene capacitor have been calculated by using the Finite Element Method (FEM) approach. A value of $n_{eff\text{-}TE}$ = 2.448634 and $n_{eff\text{-}TM}$ = 1.772773 have been obtained at $\lambda$ = 1550 nm without the graphene capacitor. Several theoretical models have been proposed in literature to study the graphene optical properties [41–43]. In particular, a closed form expression of the graphene optical conductivity that takes into account the main physical effects and factors, such as interband and intraband transitions, and also wavelength from the visible to the infrared range, temperature, chemical potential and hopping parameter has been assumed [43]. The model accuracy is confirmed by the optimal matching with numerical results obtained by other methods, such as the Kubo formula with an error < 1%, also avoiding the mathematical singularity obtained by that formulation for $hf = 2\mu_c$ ($h$ is the Planck constant, $f$ is the frequency and $\mu_c$ is the Fermi level) with a better matching with experimental results. A detailed model description has been also proposed in [23]. The relationship between the complex optical conductivity $\sigma$ and the relative permittivity $\varepsilon$ of the graphene is $\varepsilon = 1 + \mathbf{i}\cdot\sigma/\omega\varepsilon_0 t_{gr}$ where $\varepsilon_0$ is the vacuum permittivity. The anisotropy of the optical conductivity for the graphene monolayer has been taking into account to calculate the effective indices. The real and imaginary part of TE and TM effective indices (operating wavelength at 1550 nm) are reported in Fig. 2.

Both absorption losses of graphene and propagation losses in the bare waveguide are assumed to calculate the total optical losses in the Bragg grating sections with graphene capacitors. The TM mode provides low optical losses of the waveguide without graphene capacitor, while comparable losses between TE and TM modes for Bragg sections with graphene layers have been calculated, but much lower than the propagation losses in the bare waveguide for $\mu_c$ > 0.6 eV. Moreover, TM mode provides a higher index contrast in the Bragg grating (the maximum index contrast of TM mode is $\Delta n$ = 1.01 x $10^{-2}$, which is almost one order of magnitude higher than the value of TE mode), corresponding to a stronger grating strength ($\kappa$), which allows to reduce the device footprint $A$.

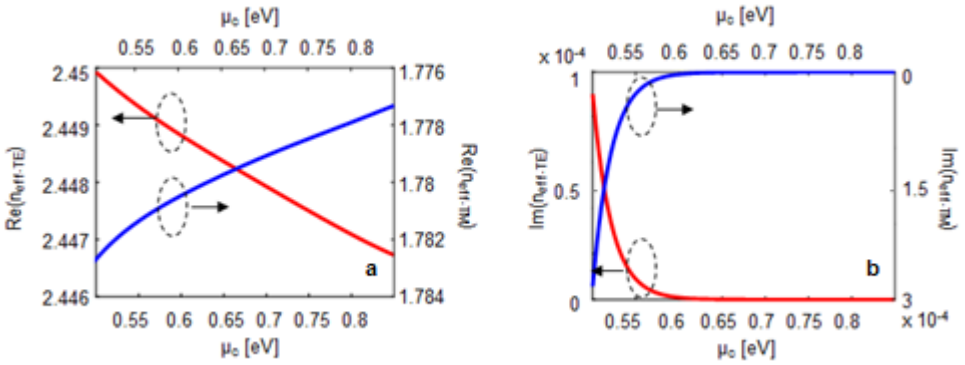


Fig. 2. Real (a) and imaginary (b) part of the effective indices in the sections with the graphene capacitor, for TE (red curve) and TM (blue curve) modes, as a function of the electrochemical potential $\mu_c$.

Therefore, assuming a TM polarization in input, a period $\Lambda$ = 1.308 μm has been chosen to operate at around 1.55 μm. Firstly, we have assumed a grating length $L_g \approx 2$ mm (number of grating periods $N$ = 1988). By Eqs. (1-3), the optical delay time spectra for several values of the chemical potential have been calculated (see Fig. 3). The slow light effect at the band-edge ensures the highest value of the optical delay time.

Optics EXPRESS

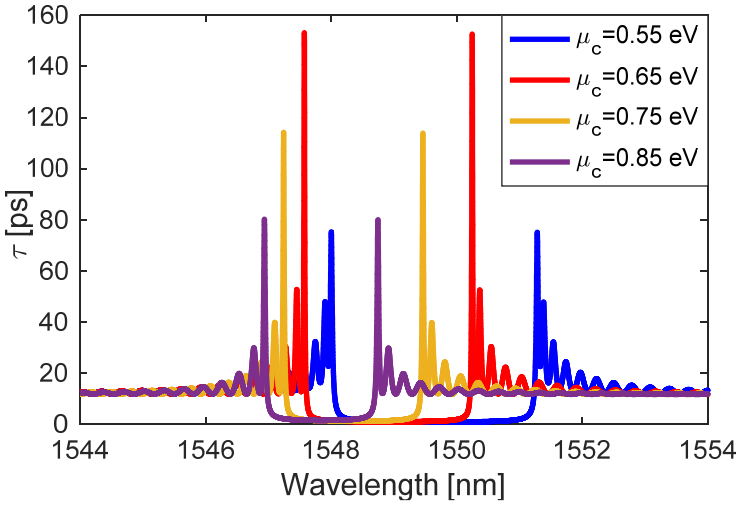


Fig. 3. Time delay spectra for several values of the electrochemical potential $\mu_c$ with $L_g$ = 2 mm.

The relationship between the electrochemical potential and the applied voltage is given by:

$$\mu_c\left(V_g\right) = \hbar v_F \sqrt{\pi \frac{C'}{e}\left|V_g - V_0\right|} \tag{4}$$

where $V_g$ is the voltage applied across the electrodes, $v_F$ is the Fermi velocity, $C'$ ( = $\varepsilon_{Al2O3}\cdot\varepsilon_0/s$) is the effective capacitance per unit area with $\varepsilon_{Al2O3}$ = 10, $e$ is the electron charge, $s$ is thickness of the alumina layer, and $V_0$ is the offset voltage referred to the natural doping ( = 0.8 V) [35]. The maximum values of the optical delay time $\tau_{max}$ as a function of the chemical potential $\mu_c$ and the applied voltage $V_g$ across the graphene electrodes are shown in Fig. 4.

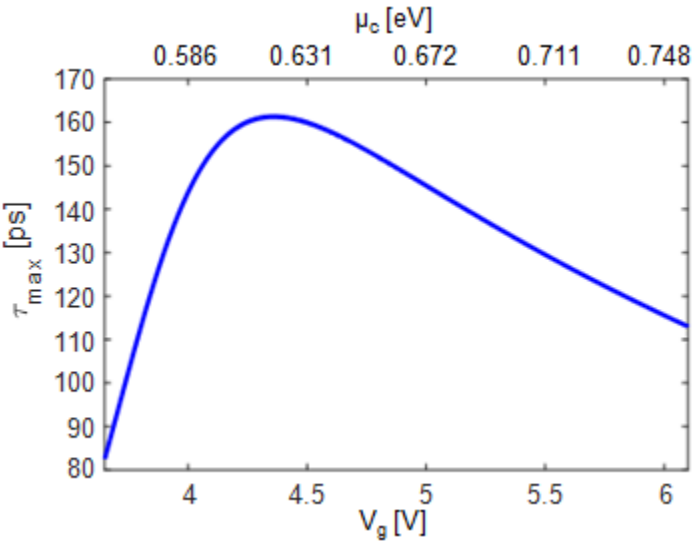


Fig. 4. Maximum delay time $\tau_{max}$ vs voltage $V_g$ and electrochemical potential $\mu_c$ with $L_g$ = 2 mm.

Optics EXPRESS

As shown in Fig. 4, a decrease of $\tau_{max}$ has been calculated for small values of $\mu_c$, because of the lower value of $Q$-factor due to higher value of optical loss. A weaker refractive index contrast has been observed with higher values of $\mu_c$ (Fig. 2a), which correspond to low values of $Q$-factor and then a worsening of $\tau_{max}$. The value of electrochemical potential $\mu_c$ = 0.619 eV, corresponding to $V_g$ = 4.363 V, provides the maximum value of the delay time $\tau_{max}$ = 161 ps, at $\lambda$ = 1547.69 nm, as shown in Fig. 5a. The group index behaviour for such value of electrochemical potential is shown in Fig. 5b. At the band-edge, the group index is maximum and then, the group velocity decrease with a consequent slow-light effect. This physical effect allows to enhance light-matter interaction, obtaining a relevant increase of the delay time.

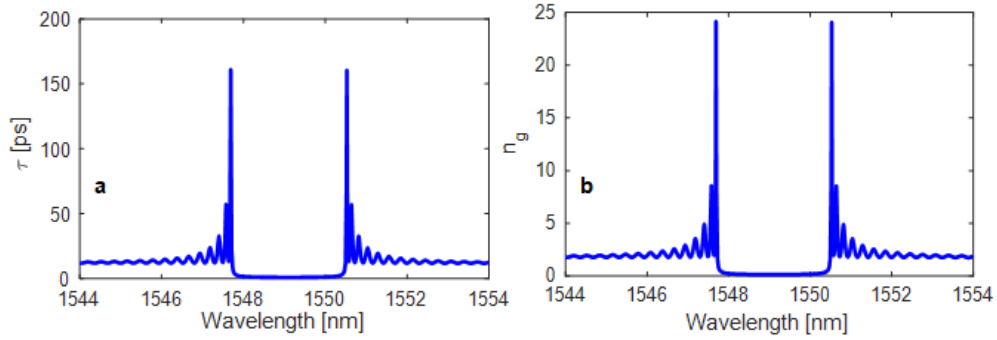


Fig. 5. (a) Delay time and (b) group index spectra of 2 mm Bragg grating, applying voltage $V_g$ = 4.363 V.

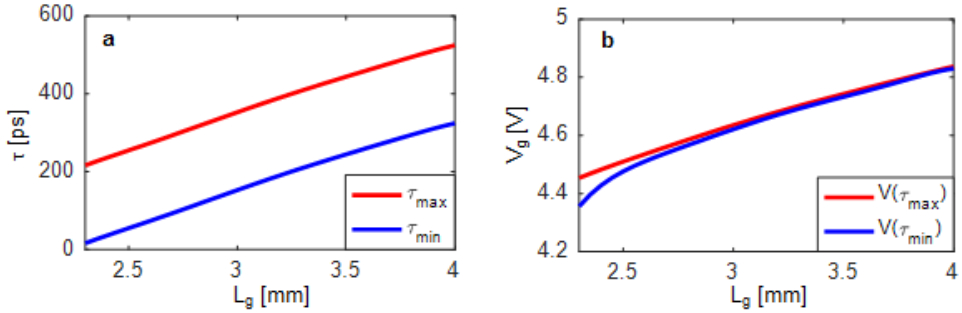


Fig. 6. (a) Behaviour of $\tau_{max}$ and $\tau_{min}$ and (b) of $V(\tau_{max})$ and $V(\tau_{min})$ as a function of the grating length $L_g$.

Assuming the same operating wavelength, the tuning of the applied voltage provides a change of the cavity performance, obtaining a minimum delay time $\tau_{min}$ = 13 ps with $V_g$ = 4.229 V. Therefore, a delay range $\Delta\tau = \tau_{max} - \tau_{min}$ = 148 ps is obtained with a length of the Bragg grating of 2 mm. In this case, the insertion loss ($IL$) is equal to 2.46 dB when $\tau = \tau_{max}$, while $IL$ = 9.72 dB has been calculated when $\tau = \tau_{min}$, corresponding to an average value $IL_{av}$ = 6.09 dB.

The optical delay line has been designed to obtain a tuning range of the delay time of 200 ps, which is a condition required for several applications in MWP (e.g. the X-band optical steering application [6]). Therefore, a parametric analysis on both the grating length and the operating voltage range has been carried out, aiming at satisfying the delay range requirement, but also to maximize both the ratio $IL_{av}/\Delta\tau$, which is usually defined as *Delay Loss* (expressed in dB/ps), and the figure of merit (*FOM*), defined as $FOM = \Delta\tau/A$ (expressed in ps/mm$^2$). We have calculated the applied voltage $V(\tau_{max})$ and $V(\tau_{min})$ corresponding to the condition of the maximum and minimum delay time, respectively, for different values of $L_g$ in order to satisfy a delay range $\Delta\tau$ = 200 ps. An increase value of $\tau_{max}$ and $\tau_{min}$ can be obtained,

Optics EXPRESS

at the expense of higher voltage values (Fig. 6). The difference between $V(\tau_{max})$ and $V(\tau_{min})$ decreases as the length increases (Fig. 6b). The feature $L_g$ = 2.3 mm corresponds to the minimum size necessary to reach $\Delta\tau$ = 200 ps.

The behaviour of the delay loss and FOM as a function of the grating length has been reported in Fig. 7a. A minimum value of delay loss has been obtained with $L_g$ = 2.6 mm, while an increase of this parameter has been observed for both larger and smaller length. As expected, the FOM decreases as the length $L_g$ increases because higher values of $L_g$ correspond to a larger area of the device, but keeping constant a delay range of 200 ps (see Fig. 7a).

For instance, with $L_g$ = 2.3 mm, $V(\tau_{max})$ - $V(\tau_{min})$ = 98.2 mV is required to ensure a delay range equal to 200 ps. As shown in Fig. 7b, the voltage shift causes a wavelength detuning $\delta$ of the order of 30 pm (operating wavelength $\lambda_0 = \lambda(\tau_{max})$ = 1547.67 nm), corresponding to high value of delay loss. For smaller voltage shifts, as $V(\tau_{max})$ - $V(\tau_{min})$ = 6.9 mV with $L_g$ = 2.9 mm, a smaller wavelength detuning $\delta$ has been calculated (~5 pm) (operating wavelength $\lambda_0 = \lambda(\tau_{max})$ = 1547.63 nm) (see Fig. 7d). In this case, the difference in *IL* corresponding to $\tau_{max}$ and $\tau_{min}$ cases is less evident, but at the same time higher optical losses have been obtained with a longer grating. Therefore, a length $L_g$ = 2.6 mm represents the best compromise because a less evident wavelength detuning is obtained if compared to the condition with shorter grating lengths, but at the same time the intrinsic optical losses are also lower by the comparison with the performance obtained with a longer device. In particular, with a length $L_g$ = 2.6 mm a low value of delay loss ( = 2.9849 x $10^{-2}$ dB/ps) and a high value of FOM = 1.54 x $10^5$ ps/mm$^2$, (see Fig. 7a) have been calculated. Higher values of FOM can be obtained for shorter length of the Bragg grating, but at the expense of a stronger delay loss.

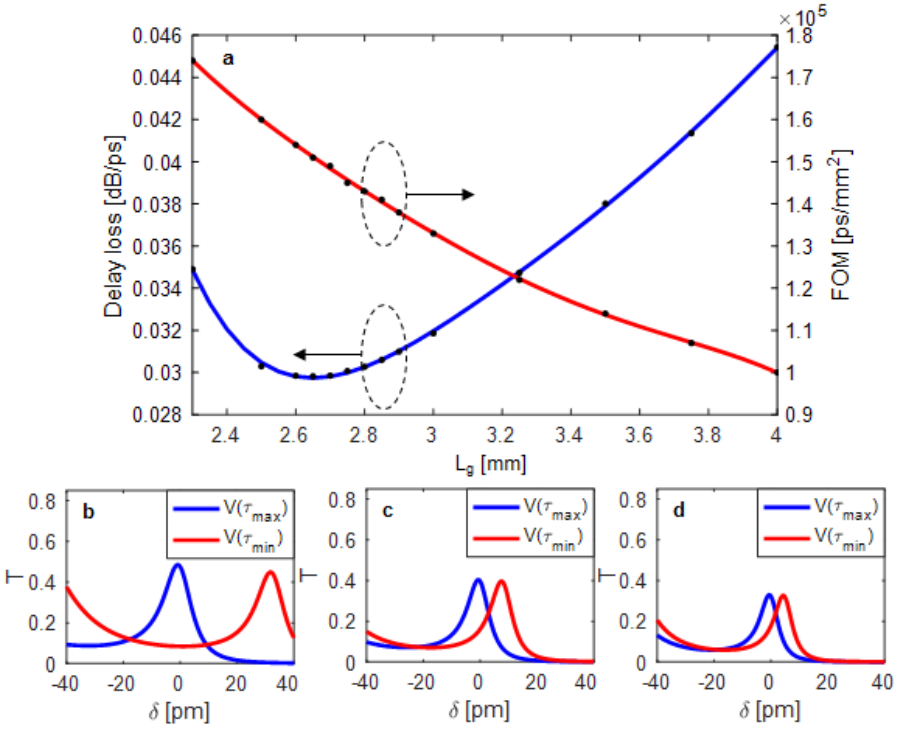


Fig. 7. (a) Delay loss (blue line) and FOM (red line) as a function of $L_g$. Transmission spectra at the band edge of the Bragg grating with (b) $L_g$ = 2.3 mm ($\lambda_0 = \lambda(\tau_{max})$ = 1547.67 nm), (c) $L_g$ = 2.6 mm ($\lambda_0 = \lambda(\tau_{max})$ = 1547.65 nm), and (d) $L_g$ = 2.9 mm ($\lambda_0 = \lambda(\tau_{max})$ = 1547.63 nm), when $V(\tau_{max})$ and $V(\tau_{min})$ are applied to the graphene electrodes.

Optics EXPRESS

The transmission spectrum and the related time delay of the Bragg grating with $L_g$ = 2.6 mm are reported in Fig. 7, taking into account an applied voltage $V_g = V(\tau_{max})$ = 4.5369 V. As shown in Fig. 8d, a maximum value delay time $\tau_{max}$ = 274 ps has been obtained with a flat and wide bandwidth ($B$ = 1.19 GHz). In particular, a bandwidth values $B$ equal to 0.085 GHz, 0.12 GHz, 0.17 GHz, 0.27 GHz have been calculated at a delay value of 0.5% $\tau_{max}$, 1% $\tau_{max}$, 2% $\tau_{max}$ and 5% $\tau_{max}$, respectively. The tuning of the delay time has been calculated by changing the applied voltage to the graphene capacitor, but assuming the same operating wavelength at $\tau = \tau_{max}$.

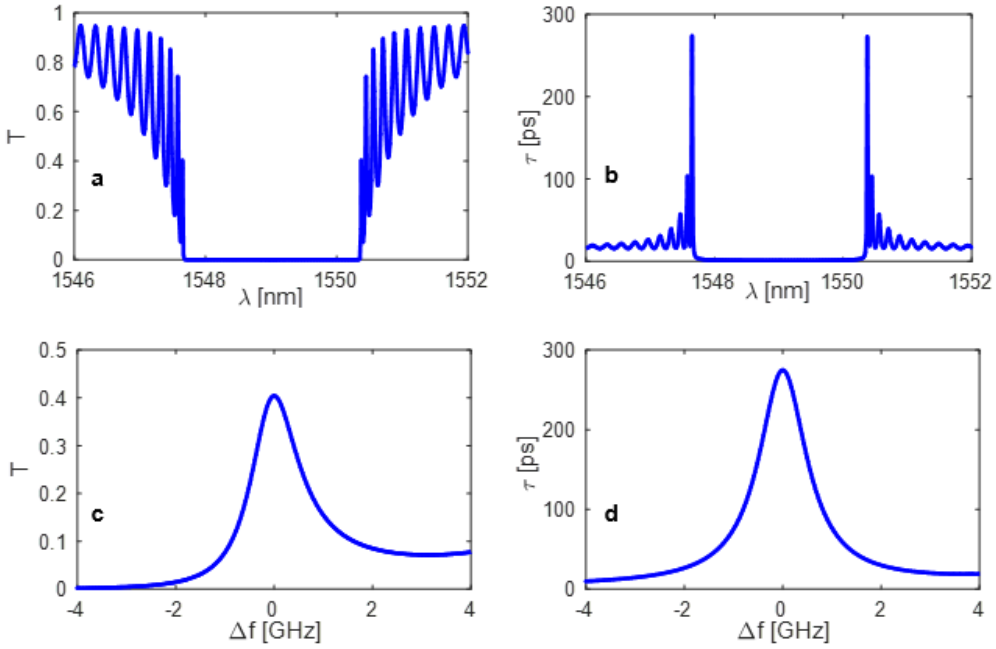


Fig. 8. (a) Transmission spectrum of the Bragg grating with $L_g$ = 2.6 mm and (b) related delay time. (c) Zoom of the transmission spectrum and (d) delay time of the first resonance peak at the band edge. Δf is the frequency shift from resonant frequency ($f_0$ ≈193.824 THz corresponding to $\lambda_0$ ≈1547.65 nm).

The delay time response as a function of $V_g$ is shown in Fig. 9. The tuning of the graphene capacitor from $V_g$ = 4.5113 V to $V_g$ = 4.5369 V, corresponding to $V(\tau_{max})$ - $V(\tau_{min})$ = 25.6 mV, allows to satisfy the delay range requirement ($\Delta\tau$ = 200 ps), obtaining $IL$ = 7.91 dB and $IL$ = 4.02 dB at $\tau_{max}$ and $\tau_{min}$, respectively. Moreover, a maximum delay range of 255.76 ps can be obtained with $L_g$ = 2.6 mm, at the expense of higher value of insertion loss up to 11.45 dB. The performance of the graphene-based Si Bragg grating with $L_g$ = 2.6 mm has been summarized in Table 1.

Optics EXPRESS

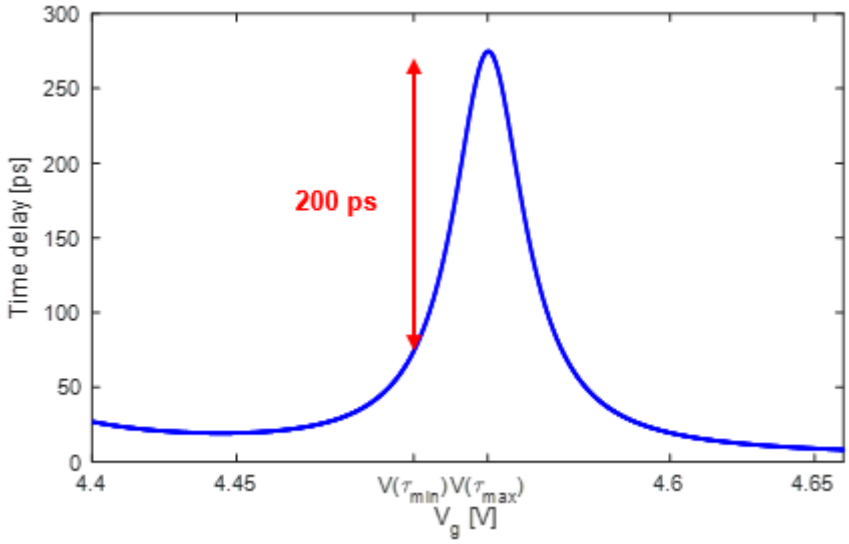


Fig. 9. Tuning of the time delay as a function of the capacitor voltage

**Table 1. Performance of the graphene-based Si Bragg grating with $L_g$ = 2.6 mm**

| $L_g$ [mm] | $A$ [mm$^2$] | $\tau_{max}$ [ps] | $\Delta\tau$ [ps] | $B$ [GHz] | Delay loss [dB/ps] | $FOM$ [ps/mm$^2$] |
|---|---|---|---|---|---|---|
| 2.60 | 1.3 x 10$^{-3}$ | 274.85 | 200 | 1.19 | 2.98 x 10$^{-2}$ | 1.54 x 10$^5$ |

The use of graphene also allows to obtain a fast switching time $t_{switch}$ and low energy consumption $P_{eff}$, in particular compared to performance achievable with other methods, such as thermo-optic tuning. We have calculated the switching energy as:

$$E_{switch} = \frac{1}{2} C \left( V(\tau_{\max})^2 - V(\tau_{\min})^2 \right) \tag{5}$$

where $C$ is the capacitance of the graphene capacitor. An area of the electrodes $A \sim (L_g/2) \cdot w_{Si}$ = 1.3 x 10$^{-3}$ mm$^2$ has been assumed, corresponding to $C$ = 8.22 pF. A value of $E_{switch}$ = 0.96 pJ and then a very high power efficiency value $P_{eff} = P_{switch}/\Delta\tau$ = 6 x 10$^{-4}$ mW/ps have been obtained assuming $V_{ON} = V(\tau_{max})$ = 4.5369 V and $V_{OFF} = V(\tau_{min})$ = 4.5113 V, and $P_{switch} = E_{switch}/t_{switch}$. The switching time $t_{switch}$ is proportional to the time constant $R_{es}C$, where $R_{es}$ is the system resistance, assumed for this configuration to be around 1 kΩ [27]. A typical value of $t_{switch}$ of about 8 ns has been calculated.

This performance confirms an improvement of the FOM compared to the state-of-the-art of integrated optical delay lines, as reported in Table 2. Such cavity provides a high $FOM$ value together with a flat bandwidth (~1.19 GHz), and also a fast switching time (8 ns). Furthermore, the value of the power efficiency is one order of magnitude less than performance reported in [15], due to the use of graphene electro-optic tuning solution. An ultra-compact footprint together with a delay range equal to 200 ps and low values of delay loss make the optical delay line very suitable for optical beamforming in Earth observation optical payloads.

Optics EXPRESS

**Table 2. State-of-the-art of optical delay lines with optical resonators.**

| | $\Delta\tau$ [ps] | $\tau_{max}$ [ps] | $B$ [GHz] | Delay loss [dB/ps] | $P_{eff}$ [mW/ps] | $t_{switch}$ [ns] | $FOM$ [ps/mm$^2$] | Tuning |
|---|---|---|---|---|---|---|---|---|
| PhCW [14] | 54 | 90 | 0.37 | 0.17 | 12.22 | - | $9.00\text{x}10^2$ | TO |
| RR + MZI [15] | 1280 | 1280 | 59 | 0.01 | 0.05 | $> 13\text{x}10^3$ | 44.5 | TO |
| CROW [18] | 800 | 800 | 6.25 | 0.01 | 5 | - | $1.14\text{x}10^2$ | TO |
| SCISSORS [19] | 345 | ~380 | 10.5 | 0.06 | 0.07 | $> 5.9\text{x}10^3$ | $7.33\text{x}10^4$ | TO |
| CROWs – SCISSORs [22] | ~200 | ~250 | - | - | - | 0.12 | $\sim 2.00\text{x}10_3$ | EO |
| Stacked–RRs [23] | 230 | 360 | > 1 | 0.1 | 0.064 | 2 | $1.44\text{x}10^5$ | EO |
| Stacked-RRs + spirals [6] | 690 | 920 | > 1 | 0.03 | 0.289 | < 2 | $1.66\text{x}10^2$ | EO |
| This work | 200 | 274 | 1.19 | 0.03 | 0.0006 | < 8 | $1.54\text{x}10^5$ | EO |

## 4. Conclusions

A graphene-based 1D Bragg grating optical delay line with a maximum time delay $\tau_{max}$ = 274 ps and a large and continuous tuning range $\Delta\tau$ = 200 ps has been designed. The delay line provides a flat bandwidth $B$ = 1.19 GHz, together with low value of delay loss 0.03 dB/ps and very small footprint ($A$ ~1.3 x $10^{-3}$ mm$^2$). The integration of a graphene capacitor enables the electro-optic continuously tuning, fast switching time ($t_{switch}$ < 8 ns) and very high power efficiency ($P_{eff}$ = 0.0006 mW/ps). Such high performance of the proposed resonant optical delay line is confirmed by the highest value of the figure of merit $FOM$ = 1.54 x $10^5$ ps/mm$^2$, which represents an improvement of the state-of-the-art of integrated optical delay lines, together with very low delay loss, high power efficiency and short time switching values. The proposed graphene-based optical delay line is very suitable for several applications in MWP and in particular for fast and low loss beam steering and beam forming of phased array antennas for telecom or Earth observation missions.